A novel model reduction approach for blisks with blend repairs and small mistuning

A Novel Model Reduction Approach for Blisks with Blend Repairs and Small Mistuning

Biao Zhou[a], Teresa Maria Berruti[b]

[a]*College of Energy and Power Engineering, Nanjing University of Aeronautics and Astronautics, 29 Yudao St., Nanjing, 210016, China*
[b]*Dipartimento di Ingegneria Meccanica e Aerospaziale, Politecnico di Torino, Corso Duca degli Abruzzi, 24, Torino, 10129, Italy*

Abstract

Blisks undergoing blade repairs by the 'blending' technique, require structural analyses to assess possible dynamic issues and also to define the blend repair limits, etc. This usually leads to prohibitive computational costs due to the large-scale full-order industrial blisk finite element models. This paper presents a novel model reduction approach, termed 'Sector Mode Assembling Reduction Technique' (SMART), for blisks with small intrinsic stiffness/geometric mistuning under blend repairs. The SMART approach starts from substructuring the full-order blisk finite element model into two kinds of components: the blended sectors with incompatible meshes and the pristine sectors with small mistuning. The truncated cyclic modes, independently computed by sector-level expansions for the two kinds of components, are strategically assembled into the SMART reduction mode basis in a sector -level form. This is beneficial for generating the reduced-order models since all the projection processes are maintained in the sector-level computations with a relatively low computational cost and memory requirement. Numerical cases demonstrate that the reduced-order models derived by the SMART approach produce structural dynamics in very good accordance with the corresponding full-order blisk finite element models, meanwhile offering the advantage of high computational efficiency and the flexibility to upgrade the reduced-order model with newly repaired blades.

Keywords: blisks, blend repair, mistuning, reduced-order model, cyclic modes

1. Introduction

Blade integrated disks (blisks) are becoming extensively used in the fan/ compressor sections of advanced aeroengines due to their reduced-weight and increased-performance benefits. However, they also suffer from notorious disadvantages of technical difficulty and high cost arising from the repair process if inevitable blade damages in service occur, e.g. foreign object damages, etc [1]. The 'blending' is the most common and cost-effective repair path for small-sized damages frequently encountered in industrial blisks. By blending out the minor damages, which are present in non-critical regions of the blade, blend repair allows to minimize the stress concentration ratio at the damaged location and at the same time to maintain the blade functionality as much as possible.

It is well known that forced responses of blisks are affected by blade mistuning that could cause one or more blades to vibrate with a significantly higher amplitude than the others. For this reason, the mistuning induced by blend repairs raises some concern. This relies on the observation that small-sized blends may notably alter both the blade frequencies and mode shapes [2], adding further mistuning to a blisk already mistuned by blade geometry variances due to manufacturing tolerance and wear, etc [3]. Recent researches therefore are focused on building high-fidelity models for blended blisks through precise geometry measurements by 3D optical scanning systems [4, 5]. They contribute to the continuing efforts on the explicit modeling and analysis of real blisks by the leading-edge digital technologies [6, 7, 8, 9, 10].

There is strong evidence that this type of high-fidelity models has an improved capability to evaluate geometric mistuning for real blisks. However, they also open up new challenges. One major drawback is that blisk models built upon the measured geometry with high-fidelity, require a high mesh density to fully capture frequency/mode variations due to blade geometric variances[11]. Such a Finite Elemet (FE) model for a real industrial blisk can contain up to several million degrees of freedom (DOFs). This requires prohibitive computational costs to perform further structural analysis in order to predict the forced response and determine the repair limits of the blend, etc.

This paper addresses a novel model reduction technique specifically for blisks that have been repaired by blending. This new reduction technique enables to generate reduced-order models (ROM) from a parent, full-order

blisk FE model which is composed of a single or multiple blended blades and a number of pristine blades with small mistuning. The small mistuning in the pristine blades could arise from the intrinsic irregularities in the material or geometric characteristics of individual blades. The former, universally modeled as the proportional perturbation of the blade stiffness matrix, is therefore referred to as stiffness mistuning. The latter, i.e., geometric mistuning due to blade geometric variances, renders simultaneous perturbation in the blade stiffness and mass matrix. It must be noticed that, the pristine blade meshes with small stiffness/geometric mistuning are supposed to possess substantially similar topology and exactly the same amount of FE nodes. Nevertheless, due to the material loss, the mesh of a typical blended blade is not topologically compatible with that of the pristine blades.

In literature there exist a number of reduction methods closely related with this research topic. They can be divided into the two categories described below.

- Component-Mode-Based Methods

The first category of reduction methods are derived from the technique of component mode synthesis (CMS). The full parent blisk model is substructured into either blade/disk components [12] or sector components [13, 14], of which the individual component normal modes are computed independently. The ROM of the full blisk is then represented by a truncated set of component modes that are assembled systematically through compatibility constraints in the component interfaces. The general substructuring step allows a straightforward integration of both small blade geometric mistuning and large blend repairs. In particular, a reduced set of principal components can be used to represent the small blade geometric variances [15, 16]. The Mode-Accelerated XXr method proposes to incorporate blend acceleration modes for bladed disks with large blends so that the size of the ROM can be lowered down [17, 18]. More recently, it is proved that the modes of a blisk with large material loss and small stiffness mistuning can be represented in terms of a subset of pseudo-nominal blisk modes[19]. The pseudo-nominal blisk is an artificially introduced blisk model with the same blade of large mistuning, nevertheless, without small stiffness in the other blades. The pseudo-nominal blisk modes are then generated by a modified CMS method.

The drawback of component-mode-based methods is the retention of a large number of component interface DOFs in the ROM. Although the interface DOFs can be reduced through a secondary modal analysis [20] or

static mode compensation [21], it still requires high computational cost that scales heavily with the number of the constraint modes. The Orthogonal Polynomial Series method was proposed to approximate the interface displacement by a linear combination of a few predefined interface modes [22]. This improvement is appealing as the constraint mode matrix is efficiently calculated in a reduced form, meanwhile the interface DOFs in the ROM drop significantly.

- System-Mode-Based Methods

In the second category, the mode basis constructed by the system-mode-based methods contains only the cyclic modes of a tuned blisk and does not require any substructuring. For blisks with small geometric mistuning, the mode basis could be expanded by incorporating the cyclic modes of the different geometrically mistuned sectors [23, 24]. In the Modified Modal Domain Analysis (MMDA) [25], the geometric variations are represented by a few Proper Orthogonal Decomposition (POD) features. The reduction basis is then constructed by a truncated cyclic modes of a 'tuned' blisk carrying a predominant POD feature. An Extension of the MMDA for blisks with large geometric mistuning is also proposed, but it requires compatible meshes among all the blades.

Large mass, stiffness or geometric mistuning with incompatible blade meshes can be handled by the PRIME method [26]. The general process involves partitioning the physical DOFs into three parts: the pristine component with small stiffness mistuning, the rogue component with large mistuning and the interface connecting the pristine and rogue components. The reduction basis is made of cyclic modes expanded to only the corresponding component DOFs. The PRIME method is computationally efficient since the mode projection is implemented in sector-level calculations [27]. A two-step projection scheme is proposed in the recently proposed partially reduced intermediate system model (PRISM) method for bladed disks with large mistuning [28]. It is reported that the PRISM saves approximately 25% computational cost compared with PRIME.

In brief, the component-mode-based methods involving the dynamic substructuring step, seem to be more convenient than the system-mode-based methods in coping with large and small geometric mistuning simultaneously. On the other hand, due to the minimal input requirement, the system-mode-based methods are generally more efficient than the component-mode-based

methods in terms of computational cost. Nevertheless, they deserve continuous research efforts particularly in incorporating small geometric mistuning in the pristine sectors in an efficient manner.

The objective of this paper is to present an original reduction approach, termed 'Sector Mode Assembling Reduction Technique' (SMART), for blisks with both blend repairs and small intrinsic stiffness/geometric mistuning. Its essential idea is to substructure the full parent blisk model into two separate components, namely, the blended sectors with incompatible meshes, and the pristine sectors with small stiffness/geometric mistuning. Physical displacement of each component can be independently approximated by different sets of cyclic modes expanded to the corresponding sectors. The cyclic modes hereafter refer to the modes pertained to either a blended sector or a nominal pristine sector with presumed cyclic symmetry at the sector interfaces. Subsequently they are assembled together to form the full blisk modes. The SMART approach can be seen as a hybrid mix of the aforementioned two categories of model reduction methods. It preserves the advantageous flexibility due to the substructuring step in the component-mode-based methods, as well as the high computational efficiency of the system-mode-based methods. Moreover, a minimal size of the final blisk ROM and easy implementation are the strong points of the SMART approach.

This paper will be organized as follows: the framework of the SMART approach is firstly outlined in Sec. 2.1 for blisks with blend repairs and small stiffness mistuning in the pristine sectors; in Sec. 2.2, the SMART is systematically extended to account for small geometric mistuning in the pristine sectors; numerical cases with comparison with the full-order FE model analysis results, are presented in Sec. 3 for validation.

2. Methodology

Consider a typical, full-order finite element model of an N-sector academic blisk in Fig. 1. It consists of a blended sector (indexed by j_b) and pristine sectors with small stiffness/geometric mistuning. Due to the material loss, the blended blade mesh is not compatible with the pristine blades, meanwhile the disk features cyclic symmetry. The frequency-domain equation of motion for the blisk under typical harmonic blade forcing is expressed in terms of the displacement $\mathbf{x}$ in the global cylindrical coordinates system:

$$\left[(1+i\gamma)\mathbf{K}-\omega^2\mathbf{M}\right]\mathbf{x}=\mathbf{f} \tag{1}$$

where $\mathbf{K}$ and $\mathbf{M}$ are full-blisk stiffness and mass matrix, respectively; γ is the structural damping ratio and $i^2 = -1$; $\mathbf{f}$ is the harmonic forcing amplitude.

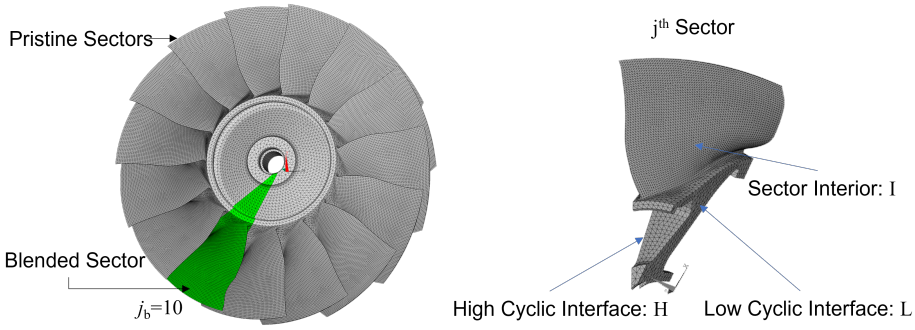

Figure 1: A full-order blisk FE model with a single blended sector (left) and index notation (right)

Provided a reduction mode basis is established as $\mathbf{\Phi}$, the displacement $\mathbf{x}$ can be projected onto the modal basis such that

$$\mathbf{x} = \mathbf{\Phi}\mathbf{q} \tag{2}$$

where $\mathbf{q}$ denotes the generalized coordinates.

The reduced system matrices and forcing term can be derived as:

$$\mathbf{M}_{\text{red}} = \mathbf{\Phi}^{\text{T}}\mathbf{M}\mathbf{\Phi}, \quad \mathbf{K}_{\text{red}} = \mathbf{\Phi}^{\text{T}}\mathbf{K}\mathbf{\Phi}, \quad \mathbf{f}_{\text{red}} = \mathbf{\Phi}^{\text{T}}\mathbf{f} \tag{3}$$

According to the notation for the physically 'isolated' j^{th} sector in Fig. 1 ($j = 1, 2, \cdots, N$), the sector-level displacement vector, modes and mass matrix in the local cylindrical coordinate system associated with each sector can be rearranged as follows:

$$\bar{\mathbf{x}}_j = \begin{bmatrix} \mathbf{x}_{j,\text{L}} \\ \mathbf{x}_{j,\text{I}} \\ \mathbf{x}_{j,\text{H}} \end{bmatrix}, \quad \bar{\mathbf{\Phi}}_j = \begin{bmatrix} \mathbf{\Phi}_{j,\text{L}} \\ \mathbf{\Phi}_{j,\text{I}} \\ \mathbf{\Phi}_{j,\text{H}} \end{bmatrix}, \quad \bar{\mathbf{M}}_j = \begin{bmatrix} \mathbf{M}_{j,\text{LL}} & \mathbf{M}_{j,\text{LI}} & \mathbf{M}_{j,\text{LH}} \\ \mathbf{M}_{j,\text{IL}} & \mathbf{M}_{j,\text{II}} & \mathbf{M}_{j,\text{IH}} \\ \mathbf{M}_{j,\text{HL}} & \mathbf{M}_{j,\text{HI}} & \mathbf{M}_{j,\text{HH}} \end{bmatrix} \tag{4}$$

where the 'bar' notation indicates sector-level quantities throughout this paper. The sector-level stiffness matrix $\bar{\mathbf{K}}_j$ and forcing vector $\bar{\mathbf{f}}_j$ are rearranged in exactly the same manner. It should be pointed out that the size of $\mathbf{x}_{j,\text{I}}$ corresponding to the physical DOFs of the sector interior nodes varies with j due to the incompatible mesh in the blended sector.

It is well recognized that the reduced system quantities in Eq. 3 can be efficiently derived by the sector-level computations with a relatively low computational cost and memory requirement (see Appendix A):

$$\mathbf{M}_{\text{red}} = \sum_{j=1}^{N} \bar{\mathbf{\Phi}}_j^{\text{T}} \bar{\mathbf{M}}_j \bar{\mathbf{\Phi}}_j, \quad \mathbf{K}_{\text{red}} = \sum_{j=1}^{N} \bar{\mathbf{\Phi}}_j^{\text{T}} \bar{\mathbf{K}}_j \bar{\mathbf{\Phi}}_j, \quad \mathbf{f}_{\text{red}} = \sum_{j=1}^{N} \bar{\mathbf{\Phi}}_j^{\text{T}} \bar{\mathbf{f}}_j \tag{5}$$

A novel approach, termed 'Sector Mode Assembling Reduction Technique' (SMART), is proposed below to construct the sector-level reduction mode basis $\bar{\mathbf{\Phi}}_j$.

2.1. Sector Mode Assembling Reduction Technique

For simplicity, only small stiffness mistuning are assumed in the pristine sectors at this stage. In essence, the SMART approach is a mixture of the component-mode-based reduction technique and the system-mode-based method reduction technique. It starts from substrcuturing the full blended blisk model into the pristine sector (P) component and blended sector (B) component, as depicted in Fig. 2. The two components share the common disk interfaces (Γ).

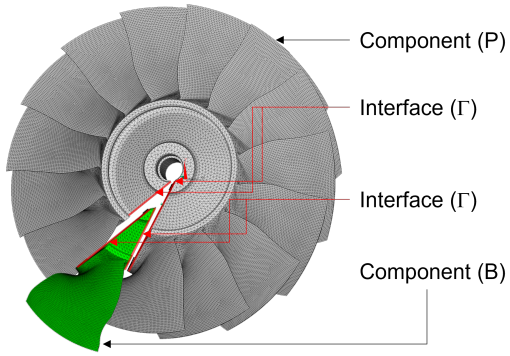

Figure 2: Substructuring of the full parent blisk model

2.1.1. Substructure reduction

The SMART proposes to project the displacement of the P component onto a truncated set of cyclic modes for a nominal sector, expanded to only the pristine sectors $\mathbf{\Phi}^{\text{P}}$ as:

$$\mathbf{x}^{\text{P}} = \mathbf{\Phi}^{\text{P}} \mathbf{q}^{\text{P}} \tag{6}$$

where $\mathbf{q}^{\mathrm{P}}$ are modal coordinates for the P component.

Eq. 6 is derived from the well-known Subset of Nominal Mode (SNM) reduction method [29], which employs the normal modes of a tuned blade disk as a reduction basis to capture the small stiffness mistuning injected into the same bladed disk. Eq. 6 is rewritten into the sector-level form in accordance with Eq. 4. Take the $j_{\mathrm{p}}^{\mathrm{th}}$ pristine sector for example:

$$\bar{\mathbf{x}}_{j_{\mathrm{p}}}^{\mathrm{P}} = \begin{bmatrix} \mathbf{x}_{j_{\mathrm{p}},\mathrm{L}} \\ \mathbf{x}_{j_{\mathrm{p}},\mathrm{I}} \\ \mathbf{x}_{j_{\mathrm{p}},\mathrm{H}} \end{bmatrix} = \begin{bmatrix} \mathbf{\Phi}_{j_{\mathrm{p}},\mathrm{L}}^{\mathrm{P}} \\ \mathbf{\Phi}_{j_{\mathrm{p}},\mathrm{I}}^{\mathrm{P}} \\ \mathbf{\Phi}_{j_{\mathrm{p}},\mathrm{H}}^{\mathrm{P}} \end{bmatrix} \mathbf{q}^{\mathrm{P}} = \bar{\mathbf{\Phi}}_{j_{\mathrm{p}}}^{\mathrm{P}} \mathbf{q}^{\mathrm{P}}, \quad j_{\mathrm{p}} \in (1, 2, \cdots, N),\ j_{\mathrm{p}} \neq j_{\mathrm{b}} \tag{7}$$

$\mathbf{\Phi}_{j_{\mathrm{p}}}^{\mathrm{P}}$ is the truncated cyclic modes $\mathbf{\Phi}^{\mathrm{P}}$ at the $j_{\mathrm{p}}^{\mathrm{th}}$ sector of a 'tuned' blisk (physically non-existent), which is composed of N nominal sectors. Note that the conceptual expansion to the full blisk mode $\mathbf{\Phi}^{\mathrm{P}}$ is not necessary. Instead, the sector-level modes $\bar{\mathbf{\Phi}}_{j_{\mathrm{p}}}^{\mathrm{P}}$ in physical coordinates can be directly expanded from the sector-level base modes $\tilde{\mathbf{\Phi}}^{\mathrm{P}}$ in cyclic coordinates for a reference nominal sector. Take the cyclic modes of harmonic index h at the $j_{\mathrm{p}}^{\mathrm{th}}$ sector for example, it reads

$$\bar{\mathbf{\Phi}}_{j_{\mathrm{p}},h}^{\mathrm{P}} = \Re[\mu_h \tilde{\mathbf{\Phi}}_h^{\mathrm{P}} e^{i(j_{\mathrm{p}}-1)h\frac{2\pi}{N}}] \tag{8}$$

where $\tilde{\mathbf{\Phi}}_h^{\mathrm{P}}$ is the complex-valued modes of harmonic index h on the reference nominal sector. It can be extracted from the cyclic modal analysis results of the reference nominal sector. μ_h is the mass-normalization mode coefficient depending on the harmonic index, i.e., $\mu_h = 1/\sqrt{N}$ for $h = 0$ and $h = N/2$ (if N is even); for the other harmonic indices, $\mu_h = \sqrt{2/N}$. The SMART approach can be technically developed based on the mode projection expressed by Eq. 6 in either the complex-valued form or the real-valued form. In this paper, since the modes $\mathbf{\Phi}^{\mathrm{P}}$ in physical coordinates are considered in the real-valued form, only the real part is kept on the right-hand side of Eq. 8.

In an analogous manner, these above operations are carried out on the B component. The displacements of the B component are approximated as:

$$\mathbf{x}^{\mathrm{B}} = \mathbf{\Phi}^{\mathrm{B}} \mathbf{q}^{\mathrm{B}} \tag{9}$$

where $\mathbf{\Phi}^{\mathrm{B}}$ stands for a truncated set of cyclic modes for the B component, and expanded to only the blended sector; $\mathbf{q}^{\mathrm{B}}$ are modal coordinates for the B component.

More concisely, the equation similar to Eq. 7 can be written at the $j_{\mathrm{b}}^{\mathrm{th}}$ sector where a blend repair occurs:

$$\bar{\mathbf{x}}_{j_{\mathrm{b}}}^{\mathrm{B}} = \begin{bmatrix} \mathbf{x}_{j_{\mathrm{b}},\mathrm{L}} \\ \mathbf{x}_{j_{\mathrm{b}},\mathrm{I}} \\ \mathbf{x}_{j_{\mathrm{b}},\mathrm{H}} \end{bmatrix} = \begin{bmatrix} \mathbf{\Phi}_{j_{\mathrm{b}},\mathrm{L}}^{\mathrm{B}} \\ \mathbf{\Phi}_{j_{\mathrm{b}},\mathrm{I}}^{\mathrm{B}} \\ \mathbf{\Phi}_{j_{\mathrm{b}},\mathrm{H}}^{\mathrm{B}} \end{bmatrix} \mathbf{q}^{\mathrm{B}} = \bar{\mathbf{\Phi}}_{j_{\mathrm{b}}}^{\mathrm{B}} \mathbf{q}^{\mathrm{B}} \tag{10}$$

where the sector-level modes $\bar{\mathbf{\Phi}}_{j_{\mathrm{b}}}^{\mathrm{B}}$ is the truncated cyclic modes of a tuned blisk carrying N duplicated blended sectors, directly expanded at the $j_{\mathrm{b}}^{\mathrm{th}}$ sector.

2.1.2. Synthesis

The reduction mode basis for the full blended blisk model is to be constructed by synthesizing the two sets of cyclic modes $\mathbf{\Phi}^{\mathrm{P}}$ and $\mathbf{\Phi}^{\mathrm{B}}$ for the P and B components respectively. Nevertheless, these original projection basis vectors are not continuous at the common sector interfaces because they are derived by two independently proceeded cyclic modal analyses. Therefore, an appropriate constraint or the displacement compatibility condition is expected to ensure the physical displacement continuity at the common sector interfaces. In this paper, physical displacement compatibility is enforced at the common interfaces Γ between the two components in Fig. 2, i.e., :

$$\bar{\mathbf{x}}_{\Gamma}^{\mathrm{B}} = \bar{\mathbf{x}}_{\Gamma}^{\mathrm{P}} \tag{11}$$

The displacement for the interface DOFs of the P component $\bar{\mathbf{x}}_{\Gamma}^{\mathrm{P}}$ can be extracted from Eq. 7 as

$$\bar{\mathbf{x}}_{\Gamma}^{\mathrm{P}} = \begin{bmatrix} \mathbf{x}_{j_{\mathrm{b}}-1,\mathrm{H}} \\ \mathbf{x}_{j_{\mathrm{b}}+1,\mathrm{L}} \end{bmatrix} = \begin{bmatrix} \mathbf{\Phi}_{j_{\mathrm{b}}-1,\mathrm{H}}^{\mathrm{P}} \\ \mathbf{\Phi}_{j_{\mathrm{b}}+1,\mathrm{L}}^{\mathrm{P}} \end{bmatrix} \mathbf{q}^{\mathrm{P}} = \bar{\mathbf{\Phi}}_{\Gamma}^{\mathrm{P}} \mathbf{q}^{\mathrm{P}} \tag{12}$$

and the displacement for the interface DOFs of the B component $\bar{\mathbf{x}}_{\Gamma}^{\mathrm{B}}$ reads from Eq. 10 as

$$\bar{\mathbf{x}}_{\Gamma}^{\mathrm{B}} = \begin{bmatrix} \mathbf{x}_{j_{\mathrm{b}},\mathrm{L}} \\ \mathbf{x}_{j_{\mathrm{b}},\mathrm{H}} \end{bmatrix} = \begin{bmatrix} \mathbf{\Phi}_{j_{\mathrm{b}},\mathrm{L}}^{\mathrm{B}} \\ \mathbf{\Phi}_{j_{\mathrm{b}},\mathrm{H}}^{\mathrm{B}} \end{bmatrix} \mathbf{q}^{\mathrm{B}} = \bar{\mathbf{\Phi}}_{\Gamma}^{\mathrm{B}} \mathbf{q}^{\mathrm{B}} \tag{13}$$

At this point, let us introduce the Interface Mode Transformation (IMT), which is one of the core points of the SMART approach. That is, the interface modes of the P component $\bar{\mathbf{\Phi}}_{\Gamma}^{\mathrm{P}}$ are assumed to be a linear combination of the interface modes of the B component $\bar{\mathbf{\Phi}}_{\Gamma}^{\mathrm{B}}$:

$$\bar{\mathbf{\Phi}}_{\Gamma}^{\mathrm{B}} \mathbf{T}_{\gamma} = \bar{\mathbf{\Phi}}_{\Gamma}^{\mathrm{P}} \tag{14}$$

where $\mathbf{T}_\gamma$ represents the transformation matrix.

This assumption is reasonable since the disk part in the full blisk model still features cyclic symmetry. The physical meaning justifying the IMT is that the modal deflections of the disk part in the two sets of cyclic modes for the P and B components exhibit high similitude. For this reason, it is recommended to retain the same number of cyclic modes n_m in Eq. 6 and Eq. 9 such that the interface mode similitude in Eq. 14 can be achieved. In this condition, $\mathbf{T}_\gamma$, a fully populated matrix of the size $n_m \times n_m$ linking the two sets of interface modes, can be readily obtained by a least squares approximate solution of Eq. 14. Notice that this does not require a huge computation effort since the interface DOFs are only a fraction of the total DOFs in each sector. The relative approximation error can be evaluated in terms of matrix norms:

$$\epsilon_\mathrm{r} = \frac{\left\| \bar{\mathbf{\Phi}}_\Gamma^\mathrm{B} \mathbf{T}_\gamma - \bar{\mathbf{\Phi}}_\Gamma^\mathrm{P} \right\|_2}{\left\| \bar{\mathbf{\Phi}}_\Gamma^\mathrm{P} \right\|_2} \tag{15}$$

Magnitudes of the relative error ϵ_r are typically of the order $o(10^{-3}) \sim o(10^{-6})$. The appropriateness of the IMT as defined in Eq. 14 is hence verified.

Combining Eq. 11 $\sim$ 14 leads to the following transformation, which represents the dependence of the two sets of modal coordinates:

$$\mathbf{q}^\mathrm{B} = \mathbf{T}_\gamma \mathbf{q}^\mathrm{P} \tag{16}$$

The SMART reduction mode basis is eventually formulated in the sector-level by assembling the truncated cyclic modes of the P and B components:

$$\bar{\mathbf{x}} = \begin{bmatrix} \bar{\mathbf{x}}_{j_\mathrm{p}}^\mathrm{P} \\ \vdots \\ \bar{\mathbf{x}}_{j_\mathrm{b}}^\mathrm{B} \end{bmatrix} = \begin{bmatrix} \bar{\mathbf{\Phi}}_{j_\mathrm{p}}^\mathrm{P} \mathbf{q}^\mathrm{P} \\ \vdots \\ \bar{\mathbf{\Phi}}_{j_\mathrm{b}}^\mathrm{B} \mathbf{q}^\mathrm{B} \end{bmatrix} = \begin{bmatrix} \bar{\mathbf{\Phi}}_{j_\mathrm{p}}^\mathrm{P} \\ \vdots \\ \bar{\mathbf{\Phi}}_{j_\mathrm{b}}^\mathrm{B} \mathbf{T}_\gamma \end{bmatrix} \mathbf{q}^\mathrm{P} = \bar{\mathbf{\Phi}}^\mathrm{SMART} \mathbf{q}^\mathrm{P} \tag{17}$$

Note that Eq. 16 resulted from the displacement compatibility condition is used to condense the dependent modal coordinates $\mathbf{q}^\mathrm{B}$. As a consequence, the sector-level cyclic modes at the j_b^th blended sector is updated as $\bar{\mathbf{\Phi}}_{j_\mathrm{b}}^\mathrm{B} \mathbf{T}_\gamma$ in the assembled mode basis $\bar{\mathbf{\Phi}}^\mathrm{SMART}$. Meanwhile, $\mathbf{q}^\mathrm{P}$ becomes the only independent generalized coordinates. Note that each column vector of $\bar{\mathbf{\Phi}}_{j_\mathrm{b}}^\mathrm{B} \mathbf{T}_\gamma$ is a linear superposition of the original cyclic modes $\bar{\mathbf{\Phi}}_{j_\mathrm{b}}^\mathrm{B}$, it indicates that the new vectors in $\bar{\mathbf{\Phi}}_{j_\mathrm{b}}^\mathrm{B} \mathbf{T}_\gamma$ fully preserve the modal characteristics pertained to the B component and they remain linearly independent. Substituting $\bar{\mathbf{\Phi}}^\mathrm{SMART}$ into Eq. 5 yields the reduced system quantities of the SMART ROM.

2.1.3. Features and advantages

The proposed SMART approach possesses multiple advantages over most of the existent component/system-mode-based methods for blisks with both large and small mistuning as listed below:

- High efficiency. The reduction mode basis $\bar{\mathbf{\Phi}}^{\mathrm{SMART}}$ has a size of n_m in the column dimension, which is the number of retained cyclic modes in the P (B) component. It gives rise to a minimal size of the SMART ROM that is able to effectively represent the full-order blisk dynamics with n_m modes. By comparison, the reduction basis by the PRIME method [26, 27] (a well-developed system-mode-based reduction method) consists of 3 sets of cyclic modes merely expanded to the corresponding pristine (P), rouge (R) and interface (I) DOFs:

$$\mathbf{\Phi}^{\mathrm{PRI}} = \begin{bmatrix} \mathbf{\Phi}^{\mathrm{P}} & \mathbf{0} & \mathbf{0} \\ \mathbf{0} & \mathbf{\Phi}^{\mathrm{R}} & \mathbf{0} \\ \mathbf{0} & \mathbf{0} & \mathbf{\Phi}^{\mathrm{I}} \end{bmatrix} \tag{18}$$

  Notice that the pristine, rogue (corresponding to the interior DOFs of the blended sector in the SMART approach), and interface physical DOFs all have separate DOFs in the modal space. Provided n_m cyclic modes are retained in the target frequency range for each cyclic mode set, the size of the PRIME ROM is 3 times larger than that of the SMART ROM.

- Easy implementation. The offline cost of the SMART is mainly composed of the two independent cyclic modal analyses for the tuned pristine sector and blended sector, respectively. The two sets of cyclic modes are assembled into the SMART mode basis by the IMT at a negligible computational cost. Moreover, the vectors in the basis $\bar{\mathbf{\Phi}}^{\mathrm{SMART}}$ are linearly independent. It implies that, in contrast to the PRIME method, no conditioning is requested afterwards to avoid the potential rank deficiency problem of the mode basis matrix.

- Versatile capability. The substructuring step in the SMART provides flexibility to account for blend repairs of different shapes, sizes and positions since the sector-level B component mode basis in $\bar{\mathbf{\Phi}}^{\mathrm{SMART}}$ can be replaced in a straightforward manner. Multiple blended sectors can also be readily incorporated into the SMART ROM. Eq. 19 exemplifies

the SMART mode basis for the blisk with blend repairs both at the $j_{\mathrm{b}_1}^{\mathrm{th}}$ and $j_{\mathrm{b}_2}^{\mathrm{th}}$ sector.

$$\bar{\mathbf{x}} = \begin{bmatrix} \bar{\mathbf{x}}_{j_{\mathrm{p}}}^{\mathrm{P}} \\ \vdots \\ \bar{\mathbf{x}}_{j_{\mathrm{b}_1}}^{\mathrm{B}_1} \\ \bar{\mathbf{x}}_{j_{\mathrm{b}_2}}^{\mathrm{B}_2} \end{bmatrix} = \begin{bmatrix} \bar{\mathbf{\Phi}}_{j_{\mathrm{p}}}^{\mathrm{P}} \mathbf{q}^{\mathrm{P}} \\ \vdots \\ \bar{\mathbf{\Phi}}_{j_{\mathrm{b}_1}}^{\mathrm{B}_1} \mathbf{q}^{\mathrm{B}_1} \\ \bar{\mathbf{\Phi}}_{j_{\mathrm{b}_2}}^{\mathrm{B}_2} \mathbf{q}^{\mathrm{B}_2} \end{bmatrix} = \begin{bmatrix} \bar{\mathbf{\Phi}}_{j_{\mathrm{p}}}^{\mathrm{P}} \\ \vdots \\ \bar{\mathbf{\Phi}}_{j_{\mathrm{b}_1}}^{\mathrm{B}_1} \mathbf{T}_{\gamma}^{\mathrm{B}_1} \\ \bar{\mathbf{\Phi}}_{j_{\mathrm{b}_2}}^{\mathrm{B}_2} \mathbf{T}_{\gamma}^{\mathrm{B}_2} \end{bmatrix} \mathbf{q}^{\mathrm{P}} = \bar{\mathbf{\Phi}}^{\mathrm{SMART}} \mathbf{q}^{\mathrm{P}} \tag{19}$$

The transformation matrices $\mathbf{T}_{\gamma}^{1}$ and $\mathbf{T}_{\gamma}^{2}$ indicate that the interface mode transformation should be carried out for the two blended sectors, respectively. A remarkable advantage of the SMART approach can be also inferred from Eq. 19, and demonstrated later: the size of $\bar{\mathbf{\Phi}}^{\mathrm{SMART}}$ remains invariant for the blisk with multiple blended sectors.

Moreover, the SMART is inherently able to capture the small stiffness mistuning in the pristine sectors. An extension of the SMART for small geometric mistuning in the pristine sectors is developed in the following section.

2.2. Extended SMART for small geometric mistuning in pristine sectors

A fundamental step in the extended SMART is to expand the mode basis $\mathbf{\Phi}^{\mathrm{P}}$ in Eq. 6 in order to capture the small geometric mistuning in the pristine sectors. This is achieved by incorporating more sets of cyclic modes for different geometrically mistuned pristine sector types [23, 24]:

$$\mathbf{x}^{\mathrm{P}} = [\mathbf{\Phi}^{\mathrm{p}_1}, \cdots, \mathbf{\Phi}^{\mathrm{p}_k}, \cdots \mathbf{\Phi}^{\mathrm{p}_{N_p}}] \begin{bmatrix} \mathbf{q}^{\mathrm{p}_1} \\ \vdots \\ \mathbf{q}^{\mathrm{p}_k} \\ \vdots \\ \mathbf{q}^{\mathrm{p}_{N_p}} \end{bmatrix} = \mathbf{\Phi}^{\mathrm{P}} \mathbf{q}^{\mathrm{P}}, \quad k = 1, 2, \cdots, N_p \tag{20}$$

where $\mathbf{\Phi}^{\mathrm{p}_k}$ stands for a truncated set of cyclic modes of a 'tuned' blisk, which is artificially created by cyclically duplicating the k^{th} geometrically mistuned pristine sector type p_k. The cyclic modes are expanded to only the pristine sectors.

Generally speaking, any pristine sector associated with a unique blade geometry should be treated as an independent sector type. It is also reported that the Principal Component (PC) Analysis [15, 16] or Proper Orthogonal

Decomposition (POD) [25] can capture the geometry variances of a group of blades by quite a few PCs or POD features. This enables to construct a reduced representation of the blade geometry variances by retaining only the predominant PCs or POD features of the blade geometries. Hence, the total number of different geometrically mistuned sector types N_p could be less or equal to the total number of pristine sectors.

It should be reminded that phase difference might appear in the independently computed cyclic modes of different sector types $\mathbf{\Phi}^{\mathrm{p}_k}$. A phase correction step is necessary to ensure their phase coherence before the cyclic mode projection in Eq. 20. In the implementation practice, the Modal Scale Factor [23] is employed to spatially rotate the original cyclic base mode pairs in the complex-valued form (see Eq. 8) such that the corrected cyclic base modes are in phase with that of a reference sector type. Details are not presented in this paper for the sake of brevity.

The physical displacement compatibility condition expressed in Eq. 11 is again set at the component interfaces Γ. It yields

$$\bar{\mathbf{\Phi}}_{\Gamma}^{\mathrm{B}}\mathbf{q}^{\mathrm{B}} = \bar{\mathbf{\Phi}}_{\Gamma}^{\mathrm{p}_1}\mathbf{q}^{\mathrm{p}_1} + \cdots + \bar{\mathbf{\Phi}}_{\Gamma}^{\mathrm{p}_k}\mathbf{q}^{\mathrm{p}_k} + \cdots + \bar{\mathbf{\Phi}}_{\Gamma}^{\mathrm{p}_{N_p}}\mathbf{q}^{\mathrm{p}_{N_p}} \tag{21}$$

where $\bar{\mathbf{\Phi}}_{\Gamma}^{\mathrm{p}_k}$ represents the interface modes corresponding to the pristine sector type p_k.

By implementing the IMTs between the interface modes of the B component $\bar{\mathbf{\Phi}}_{\Gamma}^{\mathrm{B}}$ and $\bar{\mathbf{\Phi}}_{\Gamma}^{\mathrm{p}_k}$, one can have

$$\bar{\mathbf{\Phi}}_{\Gamma}^{\mathrm{B}}\mathbf{T}_{\gamma_k} = \bar{\mathbf{\Phi}}_{\Gamma}^{\mathrm{p}_k}, \quad k = 1, 2, \cdots, N_p \tag{22}$$

The dependence between the modal coordinates $\mathbf{q}^{\mathrm{B}}$ and $\mathbf{q}^{\mathrm{p}_k}$ can be deduced by substituting Eq. 22 into Eq. 21, which is expressed as

$$\mathbf{q}^{\mathrm{B}} = \mathbf{T}_{\gamma_1}\mathbf{q}^{\mathrm{p}_1} + \cdots + \mathbf{T}_{\gamma_k}\mathbf{q}^{\mathrm{p}_k} + \cdots + \mathbf{T}_{\gamma_{N_p}}\mathbf{q}^{\mathrm{p}_{N_p}} \tag{23}$$

Similar to Eq. 17, the P and B component mode bases are assembled by

making use of the expression in Eq. 23:

$$
\begin{aligned}
\bar{\mathbf{x}} &= \begin{bmatrix} \bar{\mathbf{x}}^{\mathrm{P}}_{j_\mathrm{p}} \\ \vdots \\ \bar{\mathbf{x}}^{\mathrm{B}}_{j_\mathrm{b}} \end{bmatrix} = \begin{bmatrix} \bar{\mathbf{\Phi}}^{\mathrm{P}}_{j_\mathrm{p}} \mathbf{q}^{\mathrm{P}} \\ \vdots \\ \bar{\mathbf{\Phi}}^{\mathrm{B}}_{j_\mathrm{b}} \mathbf{q}^{\mathrm{B}} \end{bmatrix} \\
&= \begin{bmatrix} \bar{\mathbf{\Phi}}^{\mathrm{p}_1}_{j_\mathrm{p}} \mathbf{q}^{\mathrm{p}_1} + \cdots + \bar{\mathbf{\Phi}}^{\mathrm{p}_k}_{j_\mathrm{p}} \mathbf{q}^{\mathrm{p}_k} + \cdots + \bar{\mathbf{\Phi}}^{\mathrm{p}_{N_p}}_{j_\mathrm{p}} \mathbf{q}^{\mathrm{p}_{N_p}} \\ \vdots \\ \bar{\mathbf{\Phi}}^{\mathrm{B}}_{j_\mathrm{b}} \mathbf{T}_{\gamma_1} \mathbf{q}^{\mathrm{p}_1} + \cdots + \bar{\mathbf{\Phi}}^{\mathrm{B}}_{j_\mathrm{b}} \mathbf{T}_{\gamma_k} \mathbf{q}^{\mathrm{p}_k} + \cdots + \bar{\mathbf{\Phi}}^{\mathrm{B}}_{j_\mathrm{b}} \mathbf{T}_{\gamma_{N_p}} \mathbf{q}^{\mathrm{p}_{N_p}} \end{bmatrix} \\
&= \left[\begin{array}{c|c|c} \bar{\mathbf{\Phi}}^{\mathrm{p}_1}_{j_\mathrm{p}} & \cdots & \bar{\mathbf{\Phi}}^{\mathrm{p}_k}_{j_\mathrm{p}} \\ \vdots & & \vdots \\ \bar{\mathbf{\Phi}}^{\mathrm{B}}_{j_\mathrm{b}} \mathbf{T}_{\gamma_1} & & \bar{\mathbf{\Phi}}^{\mathrm{B}}_{j_\mathrm{b}} \mathbf{T}_{\gamma_k} \end{array} \cdots \left|\begin{array}{c} \bar{\mathbf{\Phi}}^{\mathrm{p}_{N_p}}_{j_\mathrm{p}} \\ \vdots \\ \bar{\mathbf{\Phi}}^{\mathrm{B}}_{j_\mathrm{b}} \mathbf{T}_{\gamma_{N_p}} \end{array}\right.\right] \begin{bmatrix} \mathbf{q}^{\mathrm{p}_1} \\ \vdots \\ \mathbf{q}^{\mathrm{p}_k} \\ \vdots \\ \mathbf{q}^{\mathrm{p}_{N_p}} \end{bmatrix} \\
&= \bar{\mathbf{\Phi}}^{\mathrm{SMART}} \mathbf{q}^{\mathrm{P}} \qquad (24)
\end{aligned}
$$

In the extended SMART approach, the size of $\bar{\mathbf{\Phi}}^{\mathrm{SMART}}$ in the column dimension becomes $n_m \times N_p$, provided that n_m cyclic modes are retained for the B component $\mathbf{\Phi}^{\mathrm{B}}$ and for each pristine sector type $\mathbf{\Phi}^{\mathrm{p}_k}$, respectively. The basis vectors in $\bar{\mathbf{\Phi}}^{\mathrm{SMART}}$ are grouped in such a way that each group of basis vectors can be interpreted as the cyclic modes for the geometrically mistuned pristine sector type p_k, coupled with the cyclic modes for the blended sector by means of the interface mode transformation.

3. Results

In this section, the SMART approach will be tested in two case studies: (1) an academic blisk FE model with a single/multiple blend repairs and small stiffness mistuning; (2) an academic blisk FE model with a single blend repair and small geometric mistuning. The SMART ROMs will be constructed to compute both the natural frequencies/modes and forced responses of the blisks under typical engine order excitations. Then these reduced-order model results will be validated against the full-order blisk model analysis results obtained in ANSYS®.

3.1. Blisk with blend repairs and small stiffness mistuning

The first case considers the academic blisk model with a single blend repair depicted in Fig. 1. The nominal blisk consists of $N = 15$ down-scaled,

low-aspect-ratio blades on a disk with simplified geometry. In Fig. 1, the 10^{th} sector has a blended blade whose mesh is incompatible with that of the pristine blades. A randomly generated blade modulus mistuning pattern is introduced into the pristine sectors as a perturbation in the elastic modulus of all the pristine blades. The blade-alone frequency (cantilevered blade frequency) variations ${}^{f}\delta_m^j$ can be calculated in terms of the mth blade mode:

$$ {}^{f}\delta_m^j = \frac{f_m^j}{f_m^{\mathrm{t}}} - 1, \quad j = 1, 2, \cdots, N \tag{25} $$

where the preceding superscript ${}^{f}(\cdot)$ stands for the frequency variation; f_m^j represents the mth blade-alone modal frequency of the jth blade; f_m^{t} is the mth modal frequency of a nominal, cantilevered blade as a reference value.

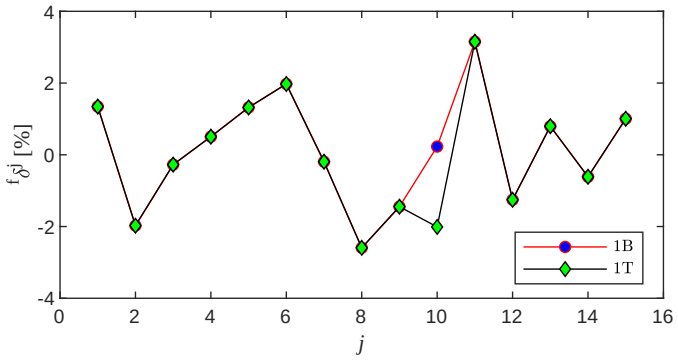

Figure 3: Blade-alone frequency variations within the blisk with a single blend repair at 10^{th} blade.

It can be seen in Fig. 3 that the blend repair and small stiffness mistuning affect the blade-alone frequencies to different extents. The 10^{th} blade frequency variation differs from mode to mode due to the geometry modification. The first bending (1B) mode frequency of the 10^{th} blade is barely affected by the blend repair, showing a frequency variation of only 0.23%. On the contrary, there is an appreciable frequency variation for the first torsional (1T) mode of blade 10, of which the frequency decreases by approximately 2% with respect to the reference value. This implies that the 1T blade mode is more sensitive to the blade geometry variations than the 1B blade mode. The frequency variation of the 1B and 1T modes is identical for each blade of the remaining sectors, since it is given by perturbed blade elastic modulus.

The SMART approach established in Sec.2.1 is implemented to generate a reduced-order model for the blisk clamped at the hub. The full-order FE model consists of 538485 quadratic tetrahedral elements with approximately 2.84×10^6 DOFs. The SMART approach starts from the cyclic mode computations for the tuned pristine sector and blended sector, respectively. The two independent cyclic modal analyses produce the superposed Frequency–Nodal diameter in Fig. 4. This research focuses on the 1B and 1T modal families of the blisk. It naturally requires that the 30 cyclic modes corresponding to the 1B and 1T modal families in Fig. 4 should be retained in the reduction mode basis as a prerequisite. In addition, it can be noticed that the modal frequencies of the 3rd blisk modal family at 0∼2ND, as well as the deformed shape of the blade part, are close to that of the blade-dominant modes with high nodal diameters (3∼7ND) in the 1T modal family. For this reason, the 5 cyclic modes corresponding to the 3rd blisk modal family at 0∼2ND in Fig. 4 are also included to ensure the adequacy of the system modal information in the reduction mode basis. As a result, totally $n_m = 35$ cyclic modes are retained for both the P and B components within the target frequency range (below 1600Hz). The two cyclic mode sets are expanded and assembled into the sector-level reduction mode basis $\bar{\mathbf{\Phi}}^{\mathrm{SMART}}$ in Eq. 17.

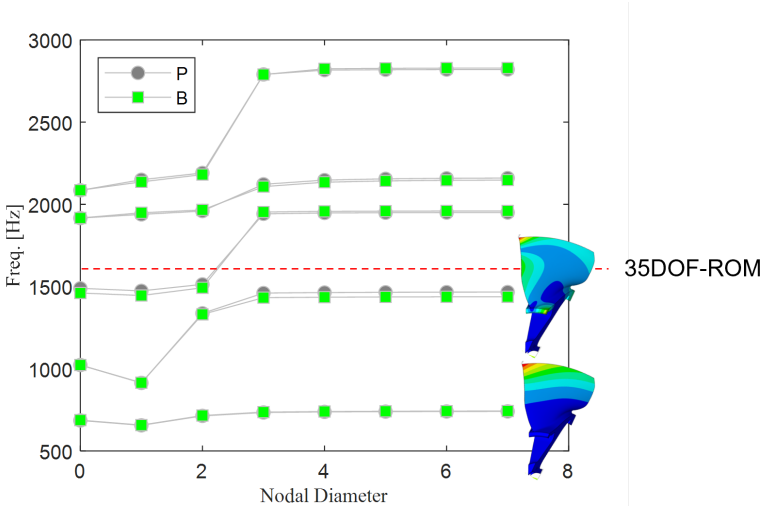

Figure 4: Frequency–Nodal diameter diagram.

The SMART ROM of the size $n_m = 35$ allows to compute the first 35 natural frequencies of the blisk. As shown in Fig. 5, the performance of

the SMART ROM is firstly evaluated by comparing its natural frequencies ('SMART') with the counterparts of the full-order blisk model ('Full'), and further examining the frequency estimation errors associated with each mode. It can be seen that the SMART ROM frequencies match very well with the full-order model predictions. All the 35 modal frequency estimation errors fall below 0.02%, which demonstrates that the SMART ROM manages to capture the natural frequencies of the parent full-order model with high accuracy.

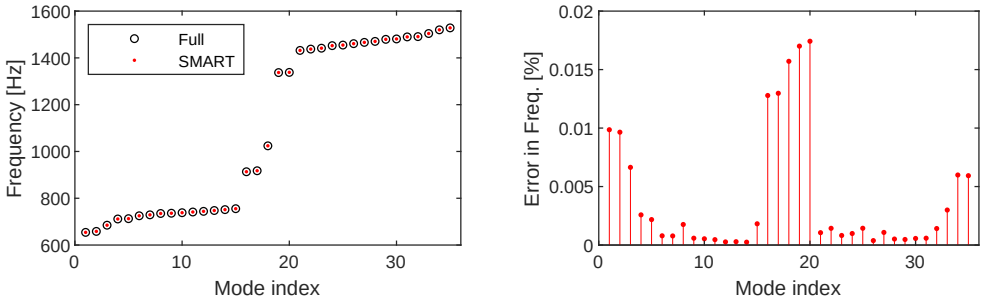

(a) natural frequencies (b) frequency estimation errors

Figure 5: Performance of SMART ROM in natural frequency prediction for the blisk with a single blended sector and small stiffness mistuning

An in-depth examination reveals that the frequency estimation errors at the full blisk mode $1 \sim 3$ and $16 \sim 20$ exhibit relatively higher values in Fig. 5b. These modes, corresponding to the more sloped parts of the graph in Fig. 5a, are characterized by more disk motion than other modes corresponding to the flatter parts in the same graph. It thus becomes obvious that the reduction mode basis for the pristine sectors $\mathbf{\Phi}^{\mathrm{P}}$ relying on the SNM method (see Eq. 6) is the reason responsible for those relatively higher frequency estimation errors. It is well known that the SNM method requires that the underlying tuned blisk modes should have closely spaced frequencies and that the modal strain energy should be primarily in the blades. As for the current case under investigation, it can be observed in Fig. 4 that the cyclic modes of the 1B and 1T mode families for the P component with low nodal diameters ($0 \sim 2$ND) are disk-dominant modes. Hence, the reduction mode basis $\mathbf{\Phi}^{\mathrm{P}}$ captures a certain number of blisk natural frequencies with less accuracy, depending on the extent to which the ideal condition for the SNM method is violated.

In addition, the SMART ROM also predicts the mistuned blisk mode shapes accurately. As can be seen in Fig. 13 where representative one-point-per-blade blisk mode shapes are depicted. By one-point-per-blade blisk mode shape, it means that the normalized modal displacement of the leading edge tip of each blade is plotted as a function of the blade index, i.e., its circumferential location on the blisk.

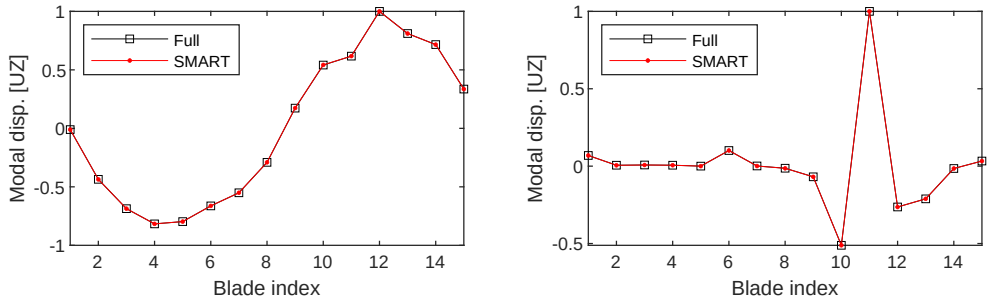

(a) Mode index 2 (b) Mode index 15

Figure 6: Performance of SMART ROM in mode prediction for the blisk with a single blended sector and small stiffness mistuning

The forced responses of the blisk under a typical engine order excitation EO = 5 are then examined. The engine order excitation consists of a number of unit nodal forces along the axial direction simultaneously applied to all the blades at the same position. The unit nodal forces are harmonic in time and differ in phase from blade to blade. A low structural damping ratio $\gamma = 0.0005$ is set for the forced response computation. The forced response amplitudes in the axial direction (UZ) at the leading edge tip of blade 10, derived from the full-order model simulation in ANSYS ('Full') and reduced-order model ('SMART'), respectively, are compared in Fig. 7. In addition, the forced response curves of a tuned blisk of the nominal design ('Nominal') are also involved. For the nominal blisk, the engine order excitation excites only those blisk modes whose number of nodal diameters meets the spatial harmonic index (engine order) of the excitation. Therefore only a single resonant peak is observed in the forced response curve around the 1B and 1T mode family, respectively. On the contrary, for the blended blisk with small mistuning, its forced response curves are featured by the clustered peaks due to the mistuning effect. Some mistuned blisk modes are strongly

excited, leading to a higher vibration level. It is clearly seen that the forced response curves denoted by 'Full' and 'SMART' are well overlapped in the frequency range of both the 1B and 1T mode families.

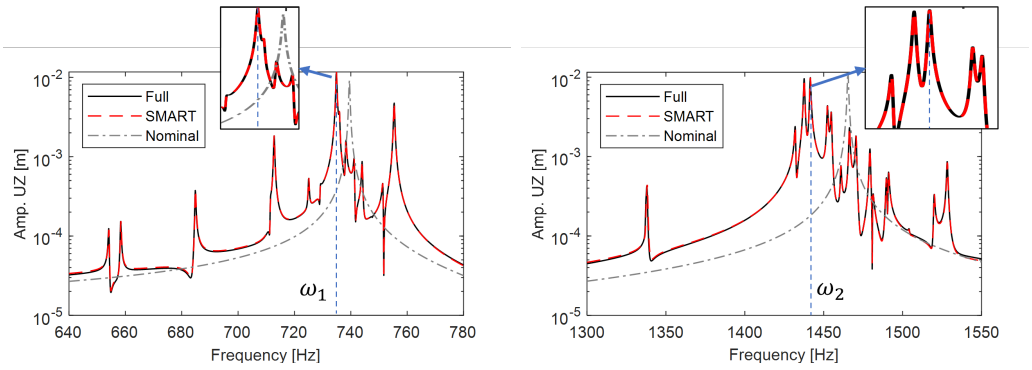

(a) around 1B mode family (b) around 1T mode family

Figure 7: Performance of SMART ROM in forced response prediction at blade 10 for the blisk with a single blended sector and small stiffness mistuning under EO = 5 excitation

Furthermore, the forced response amplitude of the leading edge tip of each blade as determined by both the full-order model simulation in ANSYS ('Full') and reduced-order model computation('SMART') for the representative resonant peaks (see the frequencies ω_1 and ω_2 in Fig. 7) is depicted in Fig. 15. Again the close-to-perfect agreement is observed. This proves that the SMART ROM is also able to accurately reproduce the forced response of the full-order blisk model.

The second case study consists in a representative full-order blisk FE model with multiple (2) blended sectors and small stiffness mistuning in the pristine sectors, as depicted in Fig. 9. It is generated by replacing the 4^{th} sector of the blisk FE model in Fig. 1 with a newly blended sector 4. That implies that only the 4^{th} sector-level mode basis needs to be recalculated and updated. A great advantage of this techinque is that, despite the inclusion of multiple blended sectors, the SMART mode basis constructed according to Eq. 19 remains of the same size in the column dimension, i.e., in this case $n_m = 35$. Fig. 10 shows that excellent agreement is also achieved between the natural frequencies derived by the full-order blisk FE model and SMART ROM, respectively. For the sake of brevity, performance of the SMART ROM

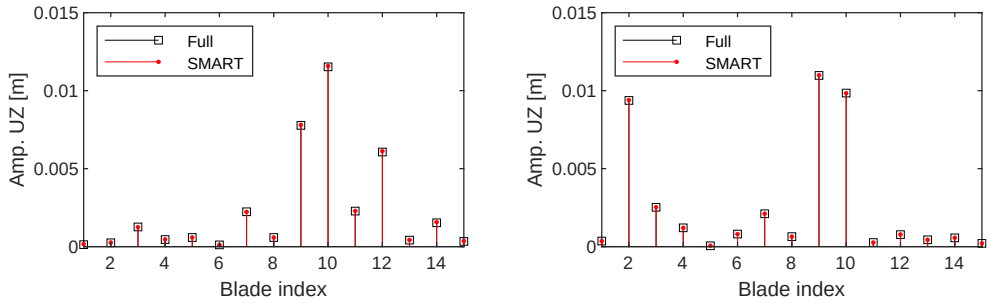

(a) blade amplitudes at ω_1 (b) blade amplitudes at ω_2

Figure 8: Performance of SMART ROM in forced response amplitude prediction at the specific resonant peaks for the blisk with a single blended sector and small stiffness mistuning under EO = 5 excitation

in forced response prediction, being very similar to the previous case study, is not shown in this case.

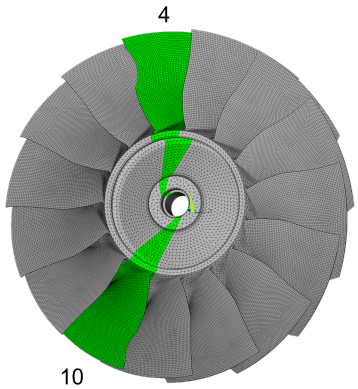

Figure 9: A full-order blisk FE model with 2 blended sectors and small stiffness mistuning.

3.2. Blisk with a blend repair and small geometric mistuning

The extended SMART elaborated in Sec. 2.2 is applied to a full-order blisk FE model with a single blend repair and small geometric mistuning in the pristine sectors, as plotted in Fig. 11. The 10^{th} blended sector is the same

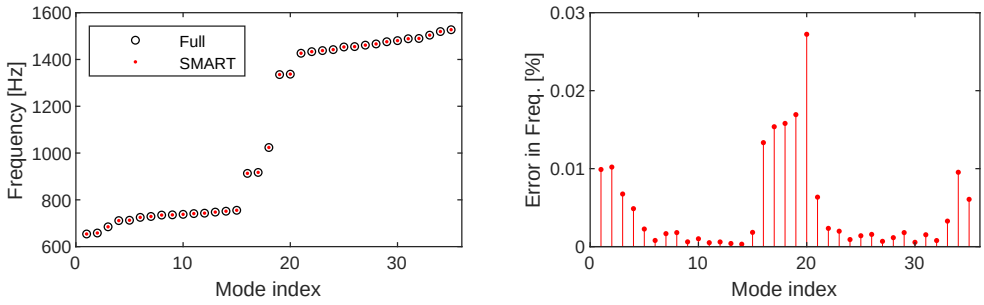

(a) natural frequencies (b) frequency estimation errors

Figure 10: Performance of SMART ROM in natural frequency prediction for the blisk with 2 blended sectors and small stiffness mistuning

as in the previous case studies. Geometric mistuning is introduced into the pristine sectors indexed by 4, 8 and 13, through scaling the nominal blade thickness by different factors. The remaining pristine sectors maintain a nominal design. This intends to represent the blade geometry variances in the pristine sectors by a reduced set of predominant PCs or POD features of the blade geometries. The blade-alone frequency variations of the geometrically modified blades with respect to the nominal blade are listed in Table 1. It can be seen that both the 1B and 1T blade-alone modal frequencies increase due to the up-scaled blade thickness.

Table 1: Blade-alone frequency variations of geometrically modified pristine blades

Blade Mode	Frequency Variations			
	nominal blade	blade 4	blade 8	blade 13
1B	-	1.70%	1.56%	0.79%
1T	-	3.57%	3.30%	1.71%

Since there are in total $N_p = 4$ different pristine sector types in this blisk FE model, the size of the SMART mode basis derived by Eq. 24 escalates to $n_m \times N_p = 140$ in the column dimension. Nevertheless, the resultant SMART ROM is able to effectively represent the dynamics of the parent model within a frequency range covering the first 35 natural frequencies. The underlying reason is that the modal information substantially involved in the expanded SMART mode basis (with the size of 140 in the column dimension) accounts

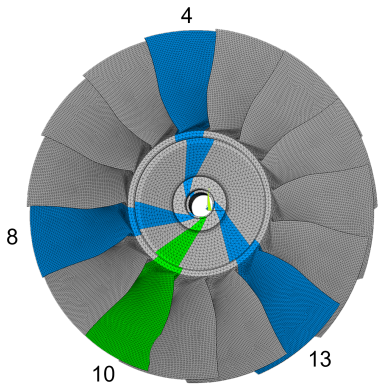

Figure 11: A full-order blisk FE model with a single blended sector and small geometric mistuning.

for merely $n_m = 35$ cyclic modes for the blended sector and $n_m = 35$ cyclic modes for each pristine sector type, respectively. Fig. 12 presents the performance of the SMART ROM in natural frequency predictions. The highest frequency estimation error increases up to 0.46%, which is still acceptable. The appreciable frequency estimation errors at the full blisk mode $1 \sim 3$ and $16 \sim 20$ are due to the intrinsic limitation of the SNM method for the reduction mode basis of the pristine sectors $\mathbf{\Phi}^{\mathrm{P}}$, as already explained in Sec. 3.1. For the same reason, the one-point-per-blade blisk mode 2 in Fig. 13a, which tends to have relatively more disk participation, computed by the SMART ROM clearly deviates from the counterpart extracted from the full-order model simulation. On the contrary, excellent agreement can be seen for the blade-dominant blisk mode 15 in Fig. 13b.

A comparison of the forced responses computed by the reduced-order model and full-order model is also carried out for the blisk under a representative engine order excitation EO = 5, as presented in Fig. 14. It can be immediately observed that the the forced response curves derived by the SMART ROM are in general well overlapped with their counterparts computed by the full-order model in the target frequency ranges. Exceptions occur around 660Hz and 1340Hz corresponding to the disk-dominant modes. These minor discrepancies arise from the systematic errors already addressed in Fig. 12. Apart from these small discrepancies limited to a few frequency ranges, it can be stated that the SMART ROM captures the dynamics of the

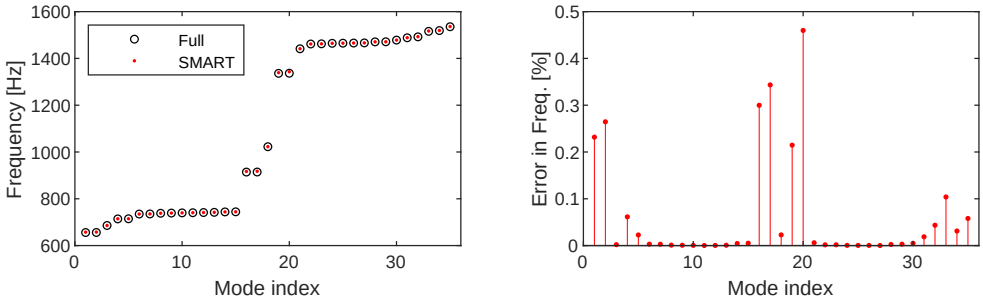

(a) natural frequencies (b) frequency estimation errors

Figure 12: Performance of SMART ROM in natural frequency prediction for the blisk with a single blended sector and small geometric mistuning

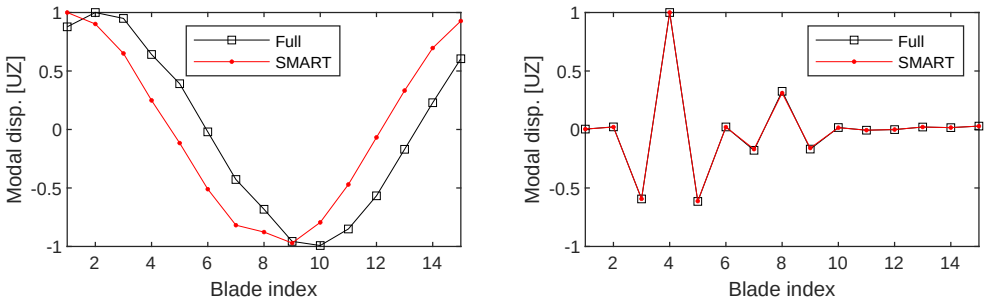

(a) Mode index 2 (b) Mode index 15

Figure 13: Performance of SMART ROM in mode prediction for the blisk with a single blended sector and small geometric mistuning

full-order blisk model with satisfactory accuracy.

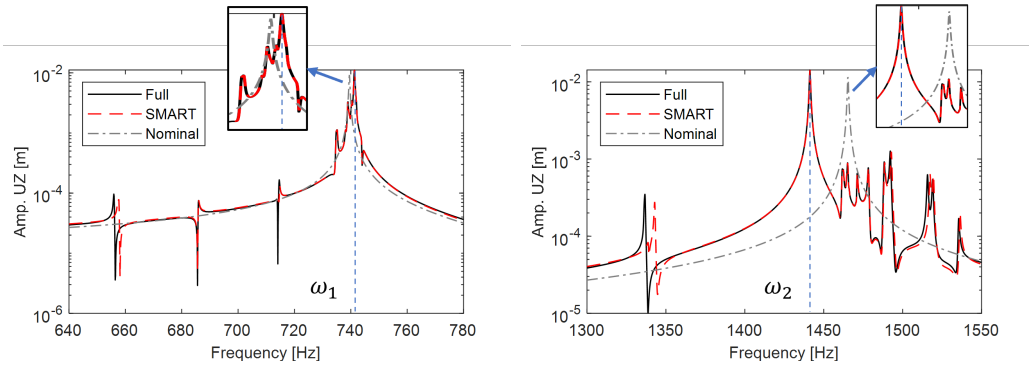

(a) around 1B mode family (b) around 1T mode family

Figure 14: Performance of SMART ROM in forced response prediction at blade 10 for the blisk with a single blended sector and small geometric mistuning under EO = 5 excitation

4. Conclusions

This paper presented a novel reduction technique, the SMART approach, taylored for blisks with the simultaneous occurrence of large geometric blade variations, such as those induced by blend repair, and small stiffness/geometric mistuning.

The SMART starts from substructuring the full-order blisk FE model into 2 components: the blended sectors with incompatible meshes and the pristine sectors with small mistuning. The truncated cyclic modes independently computed by sector-level expansions for the two components are strategically assembled into the SMART reduction mode basis in a sector-level form. This gives a great advantage for generating the reduced-order models since all the projection processes are maintained in the sector-level computations with a relatively low computational cost and memory requirement.

Comparison of results with the full-order blisk model analysis in two case studies demonstrated the satisfactory accuracy of the reduced-order models derived by the SMART approach in terms of predicting both natural frequencies and forced responses, with a substantial reduction in the computational burdens.

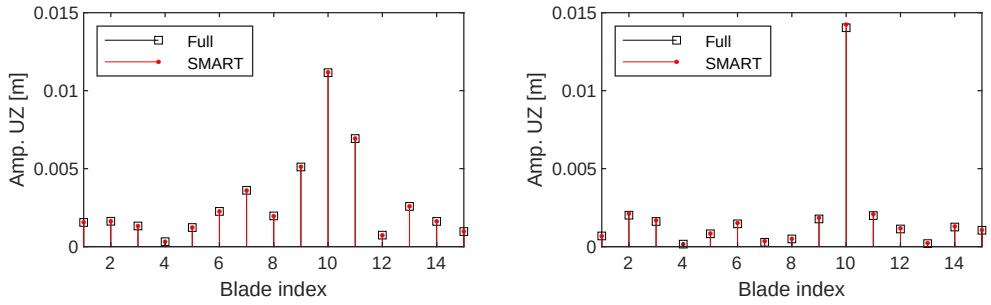

(a) blade amplitudes at ω_1 (b) blade amplitudes at ω_2

Figure 15: Performance of SMART ROM in forced response amplitude prediction at the specific resonant peaks for the blisk with a single blended sector and small geometric mistuning under EO = 5 excitation

This reduction technique is particularly suitable for assessing the impacts of blend repairs occurring in different shapes, sizes and locations, thanks to the block structure of the SMART reduction mode basis. In case that a blade is newly damaged and repaired, rather than recalculate the whole reduction mode basis, the SMART requires to only replace the corresponding sector mode block with the sector-level cyclic modes for the newly repaired sector. Moreover, the size of the reduction mode basis remains invariant for the blisk with one or multiple blended sectors.

Acknowledgements

This work has received funding from the European Union's Horizon 2020 research and innovation program under the Marie Sklodowska-Curie grant agreement No. 891197. This work is also part of a project that has received funding from National Natural Science Foundation of China (Grant No. 52175098). This support is also gratefully acknowledged.

Appendix A. Reduced Quantities by Sector-level Computations

The sector-level mass matrices $\bar{\mathbf{M}}_j$ and modes $\bar{\mathbf{\Phi}}_j$ for all the N 'isolated' sectors are gathered to form the full-blisk mass matrix and modes in the

uncoupled form:

$$\bar{\mathbf{M}} = \begin{bmatrix} \bar{\mathbf{M}}_1 & & & & \\ & \ddots & & & \\ & & \bar{\mathbf{M}}_j & & \\ & & & \ddots & \\ & & & & \bar{\mathbf{M}}_N \end{bmatrix}, \quad \bar{\mathbf{\Phi}} = \begin{bmatrix} \bar{\mathbf{\Phi}}_1 \\ \vdots \\ \bar{\mathbf{\Phi}}_j \\ \vdots \\ \bar{\mathbf{\Phi}}_N \end{bmatrix} \tag{A.1}$$

There are redundant DOFs in both the matrix $\bar{\mathbf{M}}$ and modes $\bar{\mathbf{\Phi}}$ since the adjacent sectors share common disk interfaces. The full-blisk mass matrix $\bar{\mathbf{M}}$ in the uncoupled form can be transformed into the coupled form $\mathbf{M}$, where each sector is viewed as an integral part of the entire blisk:

$$\mathbf{M} = \mathbf{E}^{\mathrm{T}} \bar{\mathbf{M}} \mathbf{E} \tag{A.2}$$

by introducing a transformation matrix $\mathbf{E}$

$$\mathbf{E} = \begin{bmatrix} \mathbf{E}_{1,a} & \mathbf{E}_{1,b} & \mathbf{0} & \cdots & \mathbf{0} \\ \mathbf{0} & \mathbf{E}_{2,a} & \mathbf{E}_{2,b} & \cdots & \mathbf{0} \\ \vdots & \vdots & \ddots & \ddots & \mathbf{0} \\ \mathbf{E}_{N,b} & \mathbf{0} & \mathbf{0} & \cdots & \mathbf{E}_{N,a} \end{bmatrix} \tag{A.3}$$

The submatrices in $\mathbf{E}$ read

$$\mathbf{E}_{j,a} = \begin{bmatrix} \mathbf{I}_{j,\mathrm{L}} & \mathbf{0} \\ \mathbf{0} & \mathbf{I}_{j,\mathrm{I}} \\ \mathbf{0} & \mathbf{0} \end{bmatrix}, \quad \mathbf{E}_{j,b} = \begin{bmatrix} \mathbf{0} & \mathbf{0} \\ \mathbf{0} & \mathbf{0} \\ \mathbf{I}_{j,\mathrm{H}} & \mathbf{0} \end{bmatrix}, \quad j \in (1, 2, \cdots, N) \tag{A.4}$$

where $\mathbf{I}_{j,\mathrm{I}}$, $\mathbf{I}_{j,\mathrm{L}}$ and $\mathbf{I}_{j,\mathrm{H}}$ are identity matrices whose sizes are determined by the total number of DOFs for the interior nodes, low and high cyclic interface nodes, respectively, in the j^{th} sector. Note that $\mathbf{E}$ is not necessarily a circulant matrix because $\mathbf{I}_{j,\mathrm{I}}$ for the blended sector might differ from that of the pristine sectors in the size.

Eq. A.2 implies only the independent DOFs, i.e., the interior DOFs and the low cyclic interface DOFs of each sector, are retained in the full-blisk mass matrix $\mathbf{M}$. The uncoupled full-blisk modes $\bar{\mathbf{\Phi}}$ are also linked with the modes $\mathbf{\Phi}$ in the coupled form as

$$\bar{\mathbf{\Phi}} = \mathbf{E}\mathbf{\Phi} \tag{A.5}$$

By substituting Eq. A.1-A.5 into Eq. 3, one can obtain the reduced mass matrix by means of sector-level computations as follows:

$$\begin{aligned} \mathbf{M}_{\text{red}} &= \mathbf{\Phi}^{\text{T}}\mathbf{M}\mathbf{\Phi} = \mathbf{\Phi}^{\text{T}}\left(\mathbf{E}^{\text{T}}\bar{\mathbf{M}}\mathbf{E}\right)\mathbf{\Phi} = \left(\mathbf{E}\mathbf{\Phi}\right)^{\text{T}}\bar{\mathbf{M}}\left(\mathbf{E}\mathbf{\Phi}\right) \\ &= \bar{\mathbf{\Phi}}^{\text{T}}\bar{\mathbf{M}}\bar{\mathbf{\Phi}} = \sum_{j=1}^{N}\bar{\mathbf{\Phi}}_j^{\text{T}}\bar{\mathbf{M}}_j\bar{\mathbf{\Phi}}_j \end{aligned} \tag{A.6}$$

The other reduced quantities in Eq. 3 can be treated in the similar fashion.

References

[1] J. Aschenbruck, R. Adamczuk, J. R. Seume, Recent progress in turbine blade and compressor blisk regeneration, Procedia CIRP 22 (2014) 256–262.

[2] B. Hanschke, A. Kühhorn, S. Schrape, T. Giersch, Consequences of borescope blending repairs on modern high pressure compressor blisk aeroelasticity, Journal of Turbomachinery 141 (2) (2019) 021002–021002–7.

[3] J. A. Beck, J. M. Brown, B. Runyon, O. E. Scott-Emuakpor, Probabilistic study of integrally bladed rotor blends using geometric mistuning models, in: 58th AIAA/ASCE/AHS/ASC Structures, Structural Dynamics, and Materials Conference, Grapevine, Texas, US, 2017.

[4] J. M. Brown, A. A. Kaszynski, D. L. Gillaugh, E. B. Carper, J. A. Beck, Optimization of airfoil blend limits with as-manufactured geometry finite element models, in: Turbo Expo: Power for Land, Sea, and Air, Vol. 84232, American Society of Mechanical Engineers, 2020, p. V011T30A029.

[5] B. Zhou, J. Zhao, N. Ye, T. M. Berruti, Blisk with small geometry mistuning and blend repair: As-measured fe model and experimental verification, in: Turbo Expo: Power for Land, Sea, and Air, Vol. In publication, American Society of Mechanical Engineers, 2022.

[6] H. Schoenenborn, D. Grossmann, W. Satzger, H. Zisik, Determination of blade-alone frequencies of a blisk for mistuning analysis based on optical measurements, in: ASME Turbo Expo 2009: Power for Land, Sea, and Air, Orlando, Florida, USA, 2009, pp. 221–229.

[7] F. Popig, P. Hönisch, A. Kühhorn, Experimental and numerical analysis of geometrical induced mistuning, in: Turbo Expo: Power for Land, Sea, and Air, Vol. 56772, American Society of Mechanical Engineers, 2015, p. V07BT32A024.

[8] A. A. Kaszynski, J. A. Beck, J. M. Brown, Automated finite element model mesh updating scheme applicable to mistuning analysis, in: Proceedings of ASME Turbo Expo 2014, Düsseldorf, Germany, 2014, p. V07BT33A025.

[9] T. Maywald, T. Backhaus, S. Schrape, A. Kühhorn, Geometric model update of blisks and its experimental validation for a wide frequency range, in: ASME Turbo Expo 2017: Turbomachinery Technical Conference and Exposition, Charlotte, North Carolina, USA, 2017, p. V07AT30A001.

[10] L. Carassale, S. Bruzzone, A. Cavicchi, M. Marrè Brunenghi, Representation and analysis of geometric uncertainties in rotor blades, in: ASME Turbo Expo 2018: Turbomachinery Technical Conference and Exposition, Oslo, Norway, 2018, p. V07CT35A025.

[11] A. A. Kaszynski, J. A. Beck, J. M. Brown, Experimental validation of a mesh quality optimized morphed geometric mistuning model, in: ASME Turbo Expo 2015: Turbomachinery Technical Conference and Exposition, Montréal, Canada, 2015, p. V07AT27A005.

[12] J. A. Beck, J. M. Brown, C. J. Cross, J. C. Slater, Component-mode reduced-order models for geometric mistuning of integrally bladed rotors, AIAA Journal 52 (7) (2014) 1345–1356.

[13] J. A. Beck, J. M. Brown, A. A. Kaszynski, E. B. Carper, D. L. Gillaugh, Geometric mistuning reduced-order model development utilizing bayesian surrogate models for component mode calculations, Journal of Engineering for Gas Turbines and Power 141 (10) (2019).

[14] J. A. Beck, J. M. Brown, A. A. Kaszynski, D. L. Gillaugh, Numerical methods for calculating component modes for geometric mistuning reduced-order models, Journal of Engineering for Gas Turbines and Power 144 (3) (2021).

[15] J. A. Beck, J. M. Brown, A. A. Kaszynski, E. B. Carper, Active subspace development of integrally bladed disk dynamic properties due to manufacturing variations, Journal of Engineering for Gas Turbines and Power 141 (2) (2018) 021001–021001–10.

[16] L. Carassale, A. Cavicchi, S. Bruzzone, M. Marrè Brunenghi, Probabilistic response of a bladed disk with uncertain geometry, Journal of Engineering for Gas Turbines and Power 141 (10) (2019).

[17] Y. Gan, J. L. Mayer, K. X. D'Souza, B. I. Epureanu, A mode-accelerated xxr (max) method for complex structures with large blends, Mechanical Systems and Signal Processing 93 (2017) 1–15.

[18] A. Lupini, B. I. Epureanu, On the use of mesh morphing techniques in reduced order models for the structural dynamics of geometrically mistuned blisks, Mechanical Systems and Signal Processing 127 (2019) 262–275.

[19] J. Gao, Y. Gao, X. Yan, K. Xu, W. Sun, Reduced order models for largely mistuned blisks with small random mistuning, AIAA Journal 58 (6) (2020) 2691–2701.

[20] P. C. Bladh R, Component-mode-based reduced order modeling techniques for mistuned bladed disks-part 1: Theoretical models, Journal of Engineering for Gas Turbines and Power 123 (1) (2001) 89–99.

[21] S.-K. Hong, B. I. Epureanu, M. P. Castanier, D. J. Gorsich, Parametric reduced-order models for predicting the vibration response of complex structures with component damage and uncertainties, Journal of Sound and Vibration 330 (6) (2011) 1091–1110.

[22] L. Carassale, M. Maurici, Interface reduction in craig–bampton component mode synthesis by orthogonal polynomial series, Journal of Engineering for Gas Turbines and Power 140 (5) (2017).

[23] M. Mbaye, C. Soize, J.-P. Ousty, A reduced-order model of detuned cyclic dynamical systems with geometric modifications using a basis of cyclic modes, Journal of engineering for gas turbines and power 132 (11) (2010).

[24] S. Baek, B. Epureanu, Reduced-order models of blisks with small geometric mistuning, Journal of Vibration and Acoustics 139 (4) (2017) 041003–041003–10.

[25] V. Vishwakarma, A. Sinha, Y. Bhartiya, J. M. Brown, Modified modal domain analysis of a bladed rotor using coordinate measurement machine data on geometric mistuning, Journal of Engineering for Gas Turbines and Power 137 (4) (2015) 042502–042502–8.

[26] A. Madden, B. I. Epureanu, S. Filippi, Reduced-order modeling approach for blisks with large mass, stiffness, and geometric mistuning, AIAA Journal 50 (2) (2012) 366–374.

[27] W. Tang, B. I. Epureanu, S. Filippi, Models for blisks with large blends and small mistuning, Mechanical Systems and Signal Processing 87 (2017) 161–179.

[28] L. Schwerdt, L. Panning-von Scheidt, J. Wallaschek, A model reduction method for bladed disks with large geometric mistuning using a partially reduced intermediate system model, Journal of Engineering for Gas Turbines and Power 143 (7) (2021).

[29] M. T. Yang, J. H. Griffin, A reduced-order model of mistuning using a subset of nominal system modes, Journal of Engineering for Gas Turbines and Power 123 (4) (2001) 893–900.